Surface Science 691 (2020) 121506

Contents lists available at ScienceDirect

Surface Science

journal homepage: www.elsevier.com/locate/susc

Surface electronic structure, relaxations and thermodynamic energies of (100), (110) and (111) surfaces of Mg_2Si: A first-principles theoretical study

Ramesh Mamindla, Manish K. Niranjan*

Department of Physics, Indian Institute of Technology, Hyderabad, TS, 502285, India

ABSTRACT

Mg_2Si is an important semiconducting silicide with several promising applications in photovoltaics, thermoelectrics, and optoelectronics. In this article, we perform a comprehensive density functional study of surface electronic structure, formation of localized surface states and their influence on relaxation and thermodynamic energies of (100), (110) and (111) surfaces of Mg_2Si. The Tran–Blaha (TB09) meta-GGA exchange-correlation (xc) functional is used in order to correctly describe the surface electronic structures and the band gaps. The band gap of bulk Mg_2Si computed using TB09 xc-functional is found to be 0.71 eV in excellent agreement with reported experimental values of 0.65–0.74 eV. Mg_2Si(100) surfaces are found to be semiconducting in contrast to previous studies wherein these surfaces were reported as metallic with zero band gaps computed using local density approximation (LDA). The surface band gap is found to be 0.32 eV for Mg-terminated (100)-(1 × 1) surface whereas it vanishes for Si-termination. However, reconstructed Si-terminated (100)-(2 × 1) surface is found to be semiconducting with band gap ~0.42 eV. The band gap for (110) surface is computed to be 0.73 eV. For (111) orientation, three different terminations are considered and are found to be semiconducting. Localized surface states are formed near valence band maximum (VBM) extending in the band gap for both (100) and (110) surfaces. In addition, localized surface gap states are also formed in the gap at ~7 eV below the VBM for Si-terminated (100) surfaces. These localized gap states are expected to have important implications for relaxations, reconstructions and thermodynamic energies of Mg_2Si surfaces. In case of (100) surfaces, interlayer relaxation is found to be significantly large for Si termination as compared to that for Mg termination. The surface energy is found to be largest for Si-terminated (100)-(1 × 1) surface with magnitude ~2.0 J/m^2. The reconstructed Si-terminated (100)-(2 × 1) surface is found to be lower in energy by ~0.2 J/m^2 than that of (100)-(1 × 1) surface. The surface energy is found to be lowest at ~0.7 J/m^2 for (111) orientations.

1. Introduction

Silicides are remarkable materials for wide variety of technological applications. For instance, metallic silicides have been widely used as low resistance contact materials in silicon based microelectronics [1–5]. Several interesting phenomena such as quantum non-Fermi liquid behavior, critical phase transition etc. arising due to strong electronic correlations have also been observed in some silicides, making them attractive for solely fundamental scientific investigations [6–8]. In recent years, semiconducting silicides with applications in thermoelectrics, photovoltaics and optoelectronics have also generated a great deal of interest [9–15]. In particular, semiconducting silicide Mg_2Si and its solid solutions have been found highly promising as thermoelectric material due to good conversion efficiency, relatively low cost and environment friendly elements [9,16–18]. Mg_2Si is an excellent material for thermoelectric power generation due to its high Seebeck coefficient, low lattice thermal conductivity and high electrical conductivity. It is also promising for applications in silicon based optoelectronics and photovoltaics owing to excellent process compatibility of silicides with standard silicon technology. Besides these applications, Mg_2Si has also been widely exploited as a reinforcing phase in aluminum and magnesium alloys for applications in aerospace and automobile industries, owing to its excellent physical and mechanical properties [19,20]. Due to their practical importance, Mg_2Si thin films and surfaces have been studied experimentally in recent years. Polycrystalline Mg_2Si thin films with (111) texture have been grown on Si (100) and Si(111) substrates by co-deposition of Mg with Si at 200 °C using molecular beam epitaxy as reported in Refs. [21,22]. Mg_2Si films have also been grown on substrates such as glass, silicon etc. using ion beam sputtering [23] and pulsed laser deposition [24]. A study of optical and thermoelectric properties of multilayer Si(111)/Mg_2Si-clusters/Si heterostructures was reported in Ref. [25]. Despite their technological importance, atomic scale ultrathin films of Mg_2Si have not been explored experimentally as well as theoretically in sufficient detail. In particular, not much is known about surface electronic structures, localized and/or resonance surface states and relative thermodynamics energies of Mg_2Si surfaces with different terminations. Here, in this article, we present a comprehensive *ab-initio* density functional (DFT) study of the surface electronic structure and relative thermodynamic stabilities of Mg_2Si surfaces with (100), (110) and (111) orientations. In particular, formation of localized surface states, surface rumpling, interlayer relaxation, surface energies and their dependence

* Corresponding author.
E-mail address: manish@iith.ac.in (M.K. Niranjan).

https://doi.org/10.1016/j.susc.2019.121506
Received 3 July 2019; Received in revised form 3 September 2019; Accepted 22 September 2019
Available online 23 September 2019
0039-6028/

on different surface orientations are explored. The surface electronic structures and band gaps are calculated using Tran–Blaha (TB09) meta-GGA [26] exchange-correlation (xc) functional. In last few years, some basic theoretical studies on Mg_2Si surfaces using DFT in combination with local density approximation (LDA) have been reported [27,28]. However, as discussed later, the use of LDA may not be adequate to describe electronic structures of Mg_2Si surfaces due to underestimation of band gaps. For instance, the present study suggests that Mg_2Si(100) surfaces are semiconducting whereas these surfaces were reported to be semi-metallic in previous reported DFT-LDA based studies [27,28]. The TB09 meta-GGA xc-functional is chosen since the band gaps computed using this scheme have been shown to be in excellent agreement with the experiments for a wide range of materials with computational cost comparable to that of conventional (semi-) local functionals [29]. We have also compared our results obtained using TB09 meta-GGA xc-functional with those obtained using Heyd–Scuseria–Ernzerhof (HSE06) hybrid functional [30] which is a more computationally expensive scheme.

The article is organized as follows. The computational methodology is presented in Section 2. Crystal and electronic structures of bulk Mg_2Si are reviewed and discussed in Section 3.1. Surface electronic structure, surface rumpling, interlayer relaxations and surface energies of (100), (110) surfaces of Mg_2Si are presented in Section 4. Finally, concluding remarks are given in Section 5.

2. Computational methodology

The surfaces are simulated using mirror-symmetric supercells with sufficient number of vacuum layers. The calculations are performed within density functional framework (DFT) [31] using formalism based on nonorthogonal pseudoatomic orbitals (PAOs) [32] basis set as implemented in the Atomistix Toolkit [33]. A basis of double-ζ PAOs including polarization functions (DZP) is used to expand Kohn–Sham wavefunctions. The Troullier–Martins norm-conserving pseudopotentials are used to describe the ionic cores [34]. Atomic positions in the supercells are relaxed using local density approximation (LDA) for xc-functional [35]. However, to compute surface electronic structures and thereby band gaps of the LDA-optimized geometries, the Tran–Blaha (TB09) meta-GGA xc-functional [26] is used. For surface electronic structure calculations, the magnitude of the *c*-parameter of TB09 meta-GGA scheme is tuned so that the computed bulk Mg_2Si band gap is matched to the experimental value ($E_{gap}^{TB09} \approx E_{gap}^{exp}$) [29]. In case of bulk Mg_2Si, the band gap is computed using TB09 meta-GGA scheme by calculating *c*-parameter self consistently. In addition to PAO formalism, the calculations are also performed using plane wave (PW) formalism and projected augmented wave (PAW) potentials [36] as implemented in the VASP package [37]. The two-dimensional (2D) Brillouin zones of surface supercells are sampled using Monkhorst–Pack $8 \times 8 \times 1$ k-point meshes. Self-consistency in the calculations is achieved by allowing total energies to converge to 10^{-6} eV/cell. The in-plane lattice parameters of the supercells are kept fixed to experimental lattice constant of bulk Mg_2Si. The out-of plane lattice parameter and atomic coordinates are relaxed until the forces on each atom become less than $\sim$0.01 eV/Å.

3. Results and discussion

3.1. Crystal and electronic structure of bulk Mg_2Si

Mg_2Si crystallizes in face centered (fcc) bravais lattice with space group symmetry *Fm*-3 m (group number: 225). The primitive cell consists one Si atom located at (0, 0, 0) and two Mg atoms at (¼, ¼, ¼) and (¾, ¾, ¾) positions. The lattice constant of Mg_2Si is computed (LDA) to be 6.319 Å and is in good agreement ($\sim$1–2%) with reported experimental value of 6.338–6.35 Å [38]. The energy bands of bulk Mg_2Si along high symmetry directions in the Brillouin zone are shown in Fig. 1a. The total and projected density of states (DOS) for Mg_2Si are shown in Fig. 1b. As can be seen in Fig. 1, the upper and lower range of valence band (VB) are primarily comprised of Si-3*p* and Mg-3*s*/2*p* orbitals respectively. The contribution to conduction band comes from Mg-3*s*/2*p* and Si-3*s* orbitals. The indirect band gap computed using LDA is found to be $\sim$0.11 eV and is smaller than reported experimental values of 0.61–0.77 eV as expected [16,21,38,39]. However, the band gap is computed to be 0.70 eV using TB09 meta-GGA xc-functional and is in excellent agreement with experimentally reported values. Fig. 2 shows the valence charge density contours on (110) surface. The Si and Mg atoms in Mg_2Si can be seen to form directional three center (Mg-Si-Mg) bonds which are mixed covalent-metallic type in nature. The charges of Si and Mg atoms in bulk Mg_2Si computed from the Mullikan population analysis are found to be 1.66 and 4.69 respectively, indicating charge transfer from Mg to Si atoms. The computed Mullikan charges of Si and Mg atoms in bulk Si and bulk Mg are 4.0 and 2.0 respectively.

3.2. Surface relaxation and electronic structure

3.2.1. Mg_2Si (100) surface

The ideal Mg_2Si(100) surface have two surface terminations as can be seen in Fig. 3. The (1 × 1) unit cell of Si-terminated surface has one Si atom, whereas (1 × 1) surface unit cell of Mg-terminated surface has two Mg atoms. Table 1 shows the computed percentage interlayer relaxation (Δd_{ij}) for both terminations. Interlayer relaxation Δd_{ij} is computed as the percentage change in separation between i^{th} and j^{th} layer as the atoms are relaxed. Interlayer relaxations arise due to reduction in coordination number of atoms and symmetry at the surface. The interlayer relaxation (Δd_{12}) for Si-termination is found to be $\sim -15\%$ which is significantly large as compared to the value ($\sim -1\%$) for Mg-termination. The negative magnitude of Δd_{12} indicates contraction or reduction in separation between top two surface layers. Overall, interlayer relaxation (Δd_{ij}) for different layers in case of Mg-termination is much smaller than that for Si terminations. The contraction of the first two top layer interspacing (Δd_{12}) for the Si-termination can be understood qualitatively from the Finnis–Heine model for surface relaxations [40] and from an ionic model which shows that surface atoms are attracted inwards due to resultant forces acting on them [41]. Table 1 also indicates a small oscillatory pattern in interlayer separation for Si-terminated surface, indicating Fridel oscillations in electron density driving the ions to relax [42]. Next, we study the electronic band structures of Si- and Mg-terminated Mg_2Si(100) surfaces. The projected bulk band structure for Si-terminated (100)-(1 × 1) surface along high symmetry lines $\bar{\Gamma} - \bar{X} - \bar{L} - \bar{\Gamma}$ is shown in Fig. 4a. The band gap of Si-terminated (100)-(1 × 1) surface computed using LDA and TB09 meta-GGA xc-functional is found to be zero. However, as reported by us recently, the Si-terminated (100)-(1 × 1) surface may undergo a (2 × 1) asymmetric dimer type of reconstruction rendering the surface semiconducting [43]. The band bap opening can be seen in Fig. 5 which shows the projected bulk band structure of reconstructed Si-terminated (100)-(2 × 1) surface along high symmetry lines $\bar{\Gamma} - \bar{X} - \bar{L} - \bar{\Gamma}$ computed using TB09 meta-GGA xc-functional. The band gap of reconstructed Si-terminated (100)-(2 × 1) surface is found to be $\sim$0.42 eV and 0.39 eV computed using TB09 meta-GGA and HSE06 hybrid xc-functional respectively. As can be seen in Fig. 4a, the surface states are formed above the valence band maximum (VBM; 0 eV) extending into the band gap as well as in the gap $\sim$7 eV below the VBM. The Fig. 4b and 4c shows the charge density (planar averaged) along the [001] direction projected on to surface bands, confirming the localization within few planes from the top surface layer. Surface localized states at $\sim$0 eV and ~ -7 eV are formed primarily by 3*p* and 1*s* orbitals of Si atoms located on top surface layer. The local density of states (LDOS) projected on first fours layers (see Fig. 6a) indicate that surface electronic structure deviate from that of bulk only for two or three layers from surface termination. Further, the average width of

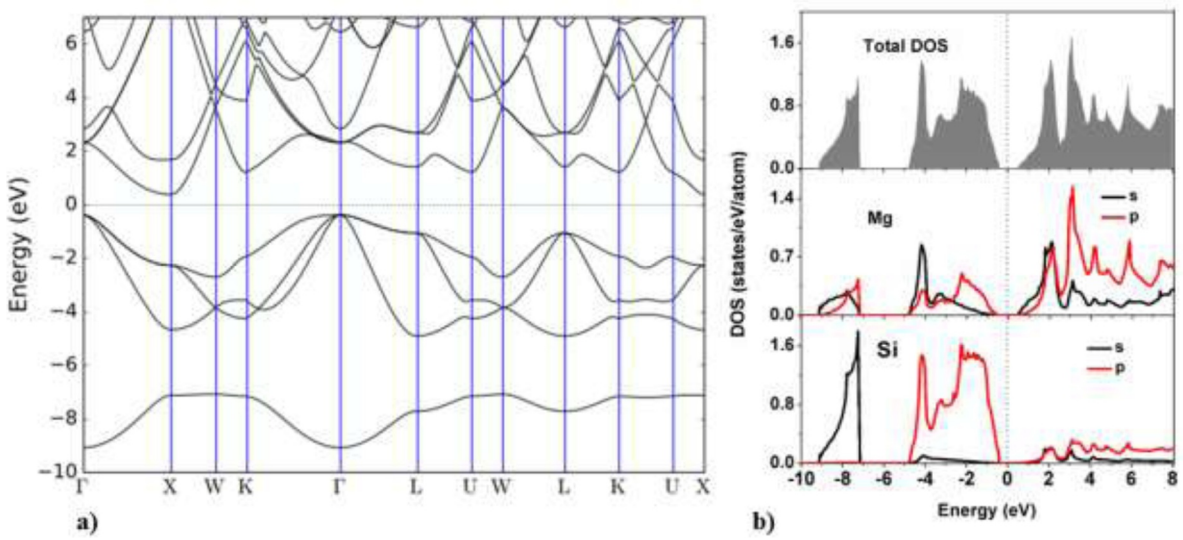

Fig. 1. (a) Energy bandstructure of bulk Mg_2Si along high symmetry directions in the Brillouin zone of face centered lattice. (b) Total density of states; partial density of states projected onto orbitals of Mg and Si atoms in bulk Mg_2Si.

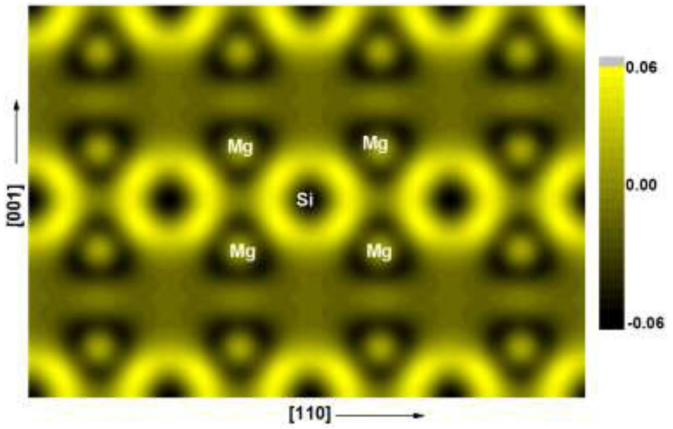

Fig. 2. Valence electron charge density contours in the (110) plane in Mg_2Si unit cell.

DOS projected on Si atoms on top surface layer is reduced as compared to that for bulk Si atoms. The reduction in the bandwidth is expected and can be understood from a simple tight binding model wherein hopping integrals are suppressed due to reduction in coordination numbers of surface atoms. The bandwidth narrowing of surface atoms is generally accompanied by band shifting toward or away from the VBM (Fermi level) which can be understood from a simple rectangular band model [44]. The Fig. 6a also shows that Si bands on top layer are shifted towards the VBM (Fermi level).

Table 1
Percentage interlayer relaxation (Δd_{ij}) for Si- and Mg-terminated (100) and (110) surfaces computed using plane wave (PW) and nonorthogonal pseudoatomic orbitals (PAO) formalisms.

	(100)-Si term		(100)-Mg term		(110)	
Interlayer	PW	PAO	PW	PAO	PW	PAO
Δd_{12}	−15.29	−15.46	−1.07	1.077	−3.39	−1.84
Δd_{23}	−2.25	5.62	−0.72	0.13	2.27	1.71
Δd_{34}	−1.17	−2.20	0.47	0.17	−2.28	−1.06
Δd_{45}	−0.45	1.64	−0.11	0.30	0.66	−0.52
Δd_{56}	−0.38	−0.70	−0.27	0.28	−1.33	−0.18
Δd_{67}	−0.20	0.32	−0.62	0.09	−0.27	0.36

Next, we discuss the electronic structure of Mg-terminated Mg_2Si (100)-(1 × 1) surface. The bulk projected band structure for Mg-termination along high symmetry lines $\bar{\Gamma} - \bar{X} - \bar{L} - \bar{\Gamma}$ is shown in Fig. 7a. The LDA computed band gap is reduced to zero. However, using TB09 meta-GGA xc-functional, the band gap comes out to be 0.32 eV. Using HSE06 scheme, the band gap is computed to be 0.51 eV. Localized

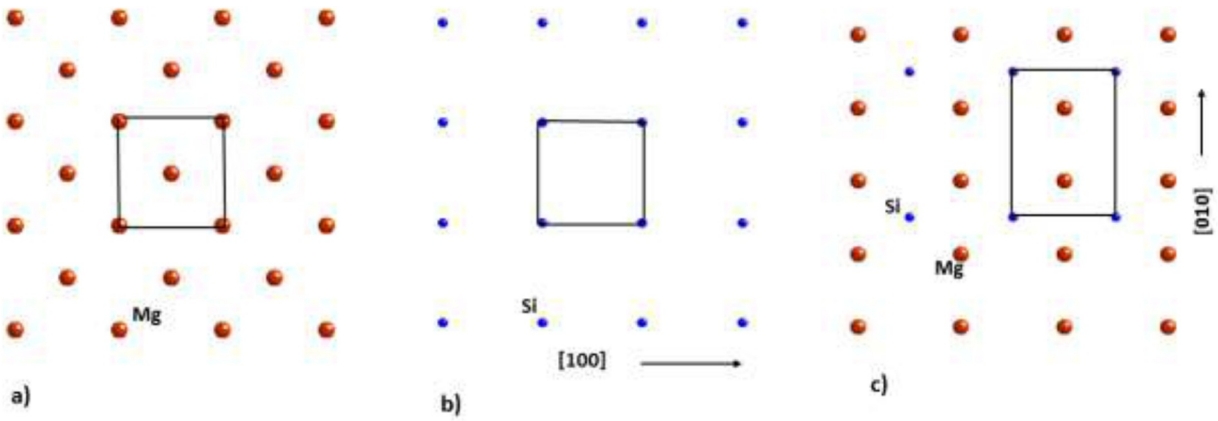

Fig. 3. Atomic arrangement on (a) Mg-terminated (b) Si-terminated (100) surfaces (c) (110) surface of Mg_2Si. Big (red) and small (blue) balls are Mg and Si atoms respectively.

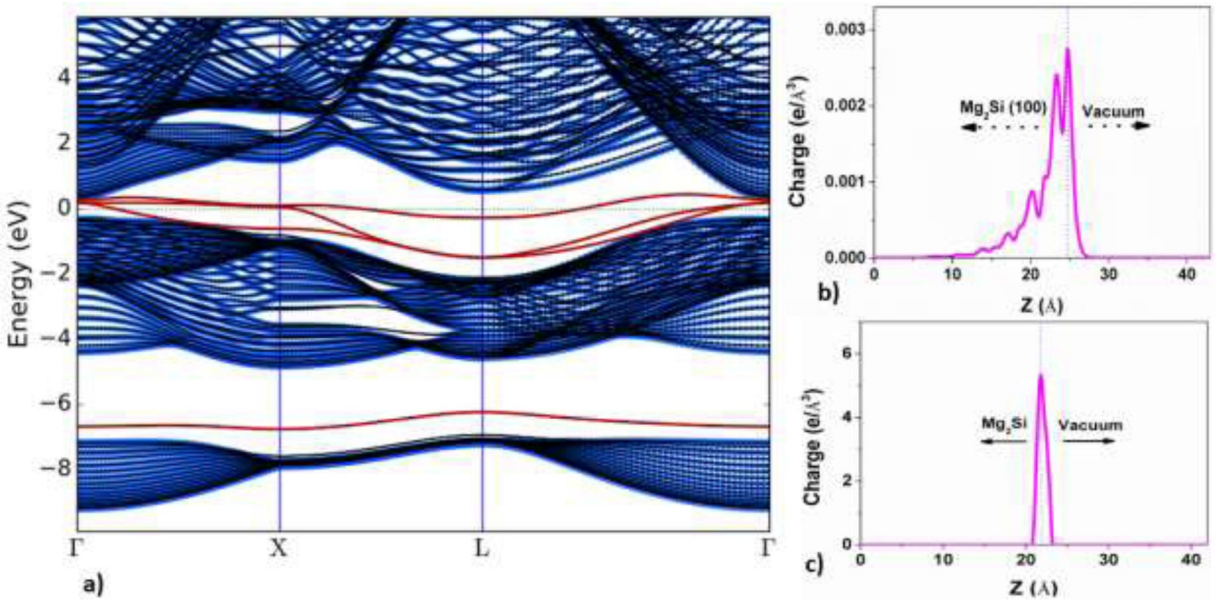

Fig. 4. (a) Projected bulk band structure of Si-terminated $Mg_2Si(100)$-(1 × 1) surfaces along $\bar{\Gamma} - \bar{X} - \bar{L}–\bar{\Gamma}$ symmetry lines in the Brillouin zone. The projected bulk bands are indicated by blue dots. Red bands indicate localized surface states. (b) Planar averaged charge density along the supercell axis for the localized bands around VBM (∼0 eV) (c) around ∼ −7 eV.

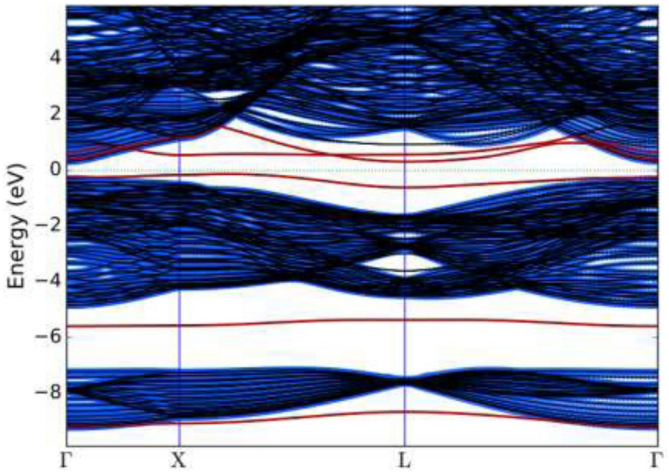

Fig. 5. Projected bulk band structure of reconstructed Si-terminated Mg_2Si (100)-(2 × 1) surfaces along $\bar{\Gamma} - \bar{X} - \bar{L}–\bar{\Gamma}$ symmetry lines in the Brillouin zone. The projected bulk bands are indicated by blue dots. Red bands indicate localized surface states.

surface states are formed in the band gap above VBM (0 eV). It may be noted that the surface state which is formed deep in valence band at ∼ −7 eV below the VBM for Si-termination is absent in case of Mg-termination. The charge density (planar averaged) projected on surface states confirms the localization of these states within few planes from the top surface layer (see Fig. 7b and c). Surface localized states around VBM (∼0 eV) are formed primarily by 3*s* orbitals of Mg atoms on top surface layer. Local density of states (LDOS) projected on first fours layers and shown in Fig. 6b, indicate that surface electronic structure deviate from that of bulk only for two layers from top layer. It may be noted from Fig. 6a and b that deviation in surface electronic structure as compared to bulk is much lesser for Mg-termination than for Si-termination. This is expected due to difference in bonding nature of surface Si and Mg atoms.

3.2.2. Mg_2Si (110) surface

Next we study surface relaxations and electronic structure of stoichiometric $Mg_2Si(110)$ surface. The (1 × 1) surface unit cell consists two Mg and one Si atoms (see Fig. 3c). Computed values of percentage interlayer relaxations (Δd_{ij}) for (110) surface are listed in Table 1. The magnitude of Δd_{12} is computed to ∼ −3.4% and is comparable to that for Mg-terminated (100) surface, but significantly smaller than that for Si-terminated (100) surface. As expected, the separation between top two surface layers is reduced. The value of Δd_{23} is ∼2% which indicates an increase in the separation between second and third layers. A small oscillatory pattern in interlayer relaxations indicating Fridel type oscillations in electron density can be inferred from values listed in Table 2. Surface rumplings (δr) resulting from unequal forces acting on the Mg and Si atoms on same layers are also computed for (110) termination. The forces acting on different type of surface atoms may differ due to difference in their atomic polarizability. The rumpling parameter is defined as the relative displacement of Mg atoms with respect to Si atoms in the surface layer and can be computed as

$$\delta r_i = (r_i^{Mg} - r_i^{Si})/d_0$$

Where d_0 is the bulk interlayer separation and $r_i^{Mg(Si)}$ are the coordinates of Mg (Si) atoms in the i^{th} layer along the supercell axis direction. Table 2 shows the computed rumpling parameters for (110) termination. The computed values of the rumpling parameter for the top three layers (δr_1, δr_2, δr_3) are ∼ −4.9%, −1.7% and 2.0%. The magnitude of rumpling parameter is highest for the top surface layer and decreases for inner layers. Further, a small oscillatory pattern in rumpling parameter can also be seen arising from Fridel type oscillations in electron density. Fig. 8 shows the projected bulk band structure for (110) termination along high symmetry lines $\bar{\Gamma} - \bar{X} - \bar{L}–\bar{\Gamma}$. The (110) surface termination is semiconducting with band gap of ∼0.73 eV and ∼0.11 eV computed using TB09 meta-GGA and LDA xc-functionals respectively. As can be seen, localized surface states are formed around VBM and conduction band minimum (CVM) extending in the band gap and in the gap at ∼7 eV below the VBM. Localization of these surface states within few planes from the top surface layer can be seen in band projected charge density (planar averaged) along the supercell axis. Surface localized states in the band gap near VBM ∼0 eV are comprised of Si-3*p* and Mg-3*s* orbitals, while those at ∼ −7 eV are comprised of 1*s* orbitals of Si atoms located on top surface layer. Local density of states (LDOS) projected on first fours layers as shown in

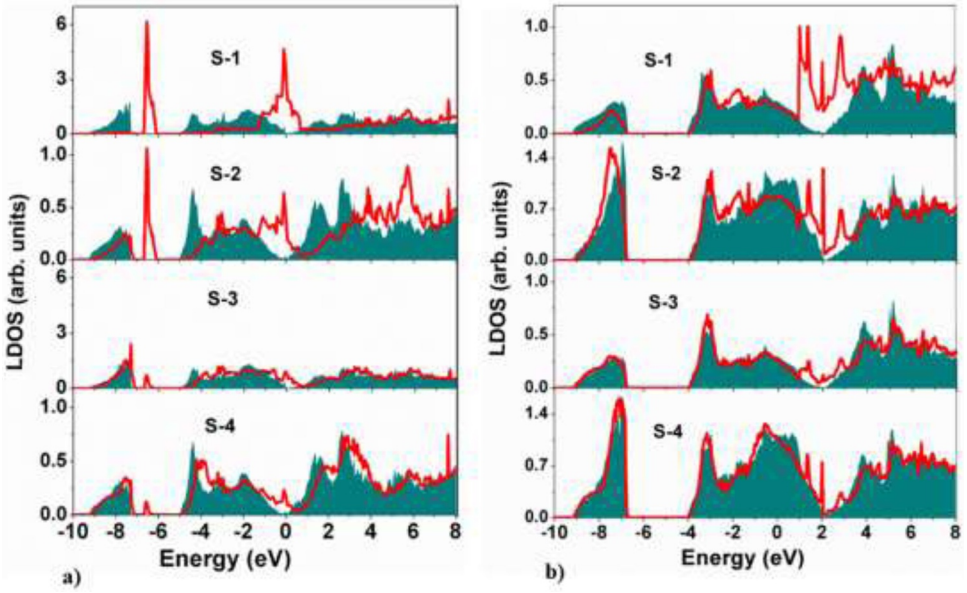

Fig. 6. Density of states (LDOS) projected on first four surface layers of (a) Si-terminated (b) Mg-terminated $Mg_2Si(100)$-(1×1) surface. The shaded plot indicates corresponding LDOS in bulk Mg_2Si.

Fig. 8b, further indicate that surface states are localized within two layers from top surface plane. Further as can be seen that unlike for (100) termination, valence bandwidth remains nearly same as that for bulk layers in case of (110) termination. This is expected as the surface is stoichiometric which leads to much smaller deviation of electronic charge density on surface layer as compared to that on bulk layers. Smaller deviation in surface electronic structure of (110) surface as compared to (100) surface is also expected as (110) termination is closed-packed while (100) termination open.

3.2.3. Mg_2Si (111) surfaces

We consider three terminations for (111) orientation as shown in Fig. 9 and refer them as A-, B- and C-terminations in the present work.

Table 2
Percentage surface rumpling (δr_i) for $Mg_2Si(110)$ surface computed using plane wave (PW) and nonorthogonal pseudoatomic orbitals (PAO) formalisms.

	PW	PAO
δr_1	−4.94	−3.77
δr_2	−1.73	−2.22
δr_3	1.97	2.00
δr_4	−1.03	−1.30
δr_5	0.73	0.75
δr_6	−0.28	−0.57

Subscript indicates the plane number.

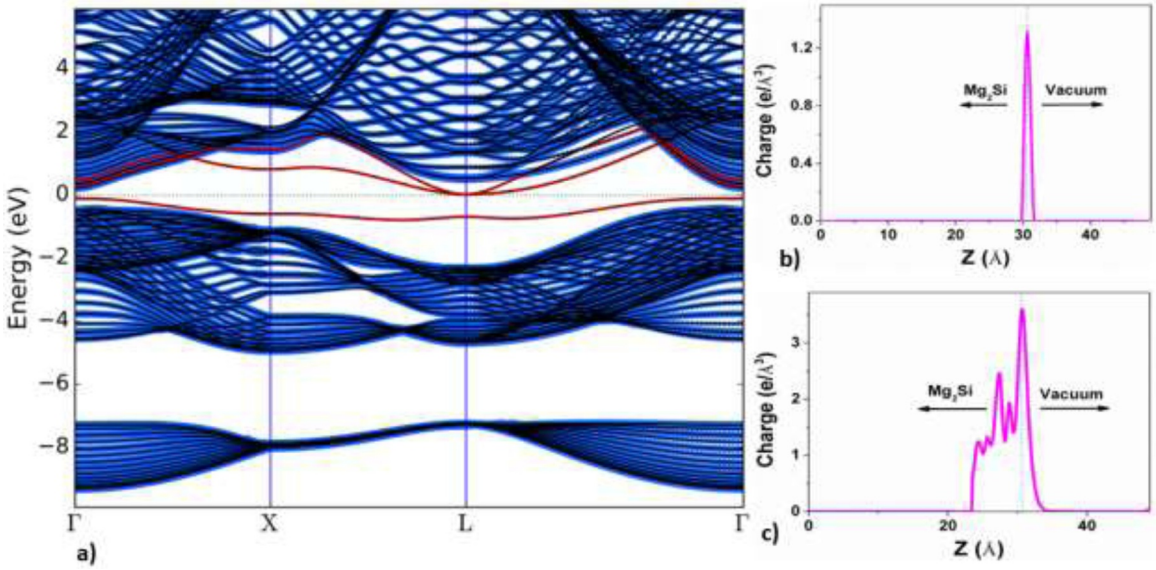

Fig. 7. (a) Projected bulk band structure of Mg-terminated $Mg_2Si(100)$surfaces along $\bar{\Gamma} - \bar{X} - \bar{L} - \bar{\Gamma}$ symmetry lines in the Brillouin zone. The projected bulk Mg_2Si bands are indicated by blue dots. Red bands indicate localized surface states. (b) Planar averaged charge density along the supercell axis for the localized bands around (b) ~0.4 eV (c) ~ −0.5 eV.

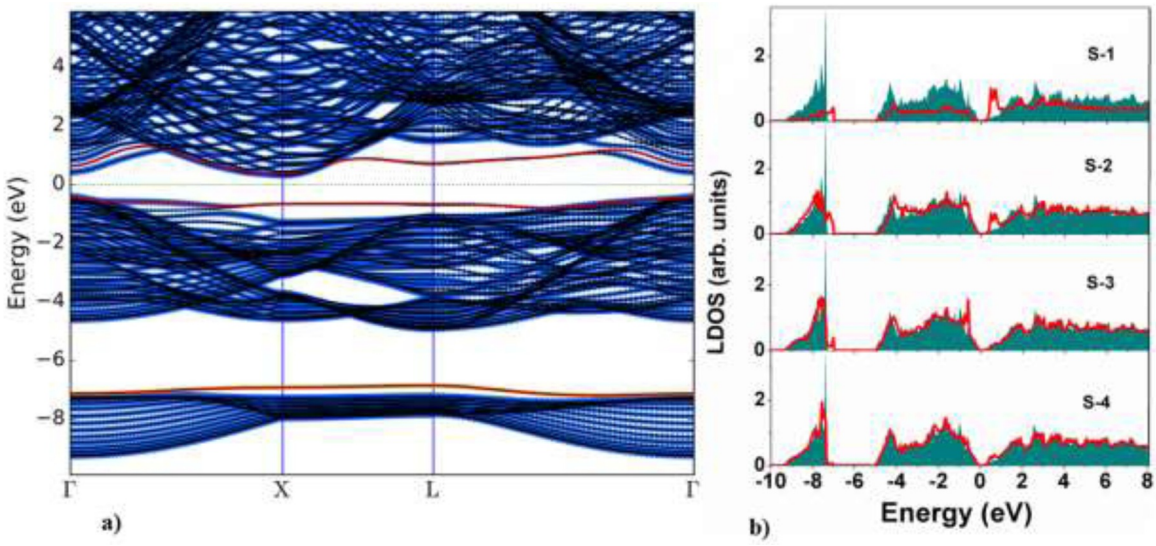

Fig. 8. (a) Projected bulk band structure of $Mg_2Si(110)$ surface along $\bar{\Gamma} - \bar{X} - \bar{L} - \bar{\Gamma}$ symmetry lines in the Brillouin zone. The projected bulk Mg_2Si bands are indicated by red dots. Red bands indicate localized surface states. (b) Density of states (LDOS) projected on first four surface layers of $Mg_2Si(110)$ supercell. The shaded plot indicates the corresponding LDOS in bulk Mg_2Si.

The hexagonal (1 × 1) surface unit cell for A-, B- and C- termination consists 1 Mg + 1 Si, 2 Mg, and 2 Mg + 1 Si atoms respectively. The computed percentage interlayer relaxations (Δd_{ij}) are found to be qualitatively similar to those obtained for (100) and (110) orientations. The projected bulk band structure along high symmetry lines for A- and B- terminations are shown in Fig. 10. The projected band structure for C- termination is found to be similar to that for A- termination. The band gaps for A-, B-, and C- terminations are found to be 0.72 eV, 0.22 eV and 0.73 eV respectively. It may be noted that no noticeable surface states are obtained in case of A- and C- terminations, whereas for B- termination, surface states are formed near VBM extending in the band gap.

4. Surface energies

In this section, we discuss the surface energies of (100), (110) and (111) orientations along with different terminations. Surface energy depends on the orientation of the surface which in turn is related to number and strength of broken bonds at the surface. In general, surface energies are expected to be higher for open surfaces than those for closed-packed surfaces. The computed energies of (100), (110) and (111) surfaces with difference terminations as a function of Mg chemical potential are shown in Fig. 11. The surface energies are calculated within Gibbs free energy formalism which has been described in several earlier reports [45–51]. The Mg rich experimental environment is indicated by the upper limit of Mg chemical potential ($\mu_{Mg} = \mu_{Mg}^{(Bulk)}$) which is scaled to 0 eV in Fig. 11. The magnitude of μ_{Mg} higher than upper limit value $\mu_{Mg}^{(Bulk)}$ indicates the formation of bulk metallic Mg on the surface. On the other hand, the magnitude of μ_{Mg} smaller than its lower limit indicate the formation of bulk Si on the surface. The Mg and Si rich conditions correspond to μ_{Mg} values near upper and lower limits respectively. As can be seen in Fig. 11, the surface energy is lowest ($\sim 0.7\ J/m^2$) for A- and C- terminated (111) surfaces. The energy for (110) orientation is calculated to be $\sim 0.9\ J/m^2$ which is lower than energies of all other surfaces but slightly higher than that for A and C-terminated (111) orientation. Further, the energy is largest for Si-terminated (100) orientation and is around $\sim 2.1\ J/m^2$ which is expected due to relatively stronger Si broken bonds at the surface. The energy of reconstructed Si-terminated (100)-(2 × 1) surface is found to be lower by $\sim 0.21\ J/m^2$ than that of relaxed (100)-(1 × 1) surface. Fig. 11 also shows that energies of Mg-terminated (100) and B-terminated (111) orientations are comparable. The computed energies of Mg_2Si surfaces may be compared with reported experimental values of Mg and Si surfaces since experimental Mg_2Si surface energies have not been reported to best of our knowledge. The reported energies of Mg(0001) and Si(111) surfaces lie in the range of 0.76–0.79 J/m^2 and 1.36–1.74 J/m^2 [52,53]. As may be noted, the computed Mg_2Si surface energies are comparable with reported energies of Mg and Si surfaces.

5. Conclusion

Density functional calculations are performed to explore (100), (110) and (111) surfaces of Mg_2Si with (1 × 1) periodicity. In particular, surface electronic structure, formation of localized surface states, surface relaxations and thermodynamic energies of (100), (110) and (111) surfaces are explored. The surface electronic structures and thereby surface band gaps are obtained using Tran–Blaha (TB09) meta-GGA xc-functional. The band gap of bulk Mg_2Si is computed to be

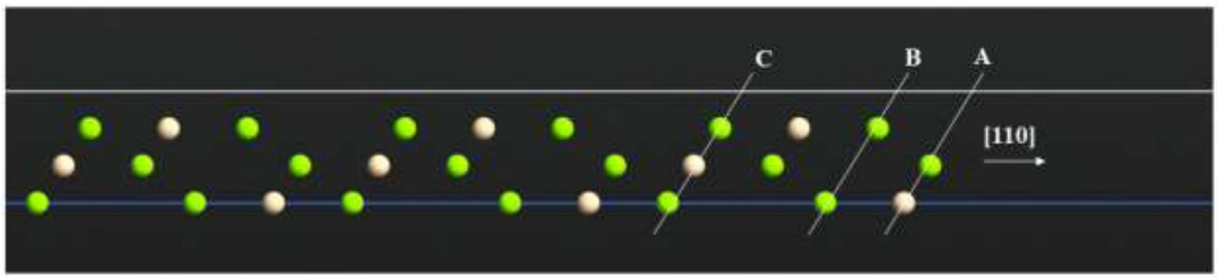

Fig. 9. $Mg_2Si(111)$ supercell with A-, B-, and C-type terminations.

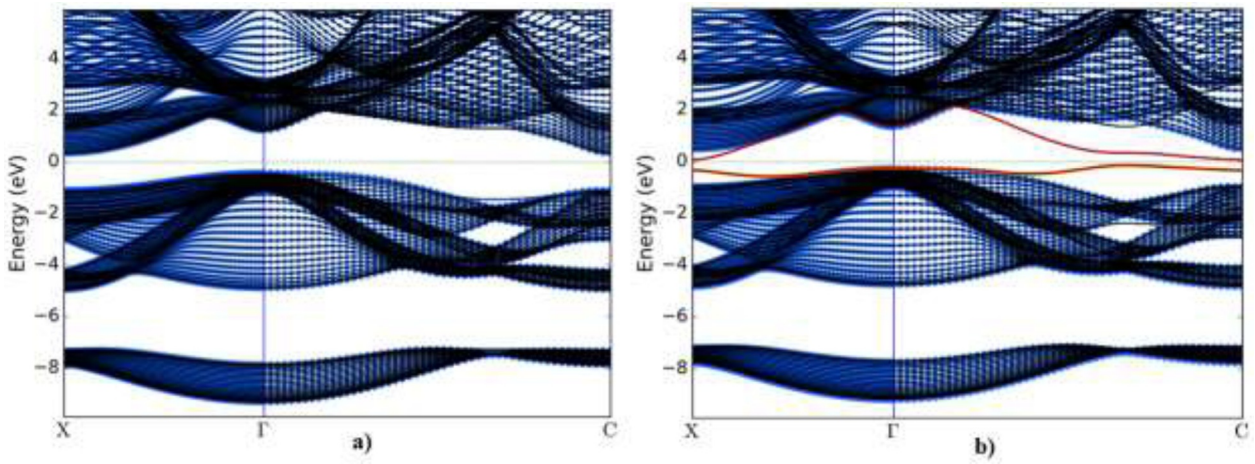

Fig. 10. (a) Projected bulk band structure of $Mg_2Si(111)$ surface along high symmetry lines in the Brillouin zone for (a) A-termination (see Fig. 8) (b) B-termination. The projected bulk Mg_2Si bands are indicated by blue dots. Red bands indicate localized surface states.

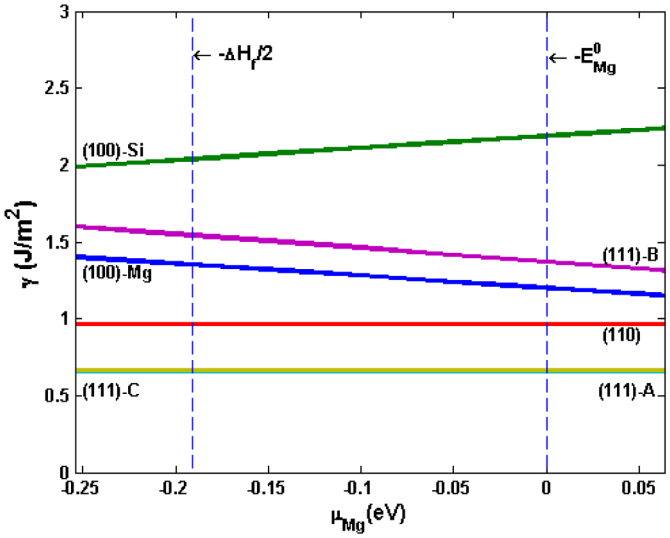

Fig. 11. Computed energies of Mg-terminated (100), Si-terminated (100), (110), A-, B- and C-terminated (111) surfaces of Mg_2Si. The upper and lower limits of Mg chemical potential (μ_{Mg}) are indicated by dashed vertical lines.

0.70 eV using TB09 meta-GGA xc-functional, which is in excellent agreement with reported experimental values. $Mg_2Si(100)$ surfaces are found to be semiconducting whereas these surfaces were reported as metallic in previous DFT + LDA based studies. The band gap of Si-terminated (100) surface is reduced to zero, whereas it is computed to be 0.32 eV for Mg-terminated (100) surface. The band gap of Si-terminated (100)-(1 × 1) surface is found to be reduced to 0 eV. However, the Si-terminated (100) surface undergoes a (2 × 1) reconstruction and exhibits a band gap of 0.42 eV. For (110) orientation, the band gap is computed to be 0.73 eV. Localized surface states are seen to be formed near VBM extending in the band gap for (100) and (110) orientations. However, for Si-terminated (100) surface, localized surface gap states are also formed in the gap at ~7 eV below the VBM. Interlayer relaxation is found to be significantly large for Si terminated (100) surface as compared to Mg terminated (100) surface. The surface energy is found to be lowest for A- and C-terminated (111) surfaces, whereas it is largest for the Si-terminated (100) surface. The energy of reconstructed Si-terminated (100)-(2 × 1) surface is computed to be lower by ~0.21 J/m^2 than that of relaxed (100)-(1 × 1) surface. We hope that the results presented in this study will stimulate further experimental and theoretical studies of Mg_2Si surfaces.

References

[1] S. Zhang, M. Ostling, Metal silicides in CMOS technology: past, present, and future trends, Crit. Rev. Solid State Mat. Sci. 28 (1) (2003).
[2] S.P. Murarka, Silicides for VLSI Applications, Academic Press, 1983.
[3] S.M. Sze, Physics of Semiconductor Devices, second ed, Wiley, New York, 1981.
[4] Silicide Technology for Integrated Circuits, in: L.J. Chen (Ed.), Silicide Technology for Integrated Circuits, IEE, London, 2004.
[5] R.T. Tung, The physics and chemistry of the Schottky barrier height, Appl. Phys. Rev. 1 (2014) 011304.
[6] P.S. Riseborough, Heavy fermion semiconductors, Adv. Phys. 49 (2000) 257–320.
[7] C Pfleiderer, D. Reznik, L. Pintschovius, H. von Lohneysen, M. Garst, A. Rosch, Partial order in the non-Fermi-liquid phase of MnSi, Nature 427 (2004) 227–231.
[8] C. Pfleiderer, S.R. Julian, G.G. Lonzarich, Non-Fermi-liquid nature of the normal state of itinerant-electron ferromagnets, Nature 414 (2001) 427–430.
[9] Semiconducting Silicides, in: V.E. Borisenko (Ed.), Semiconducting Silicides, Springer, Berlin, 2000.
[10] D.M. Rowe, CRC Handbook of Thermoelectrics, CRC Press, Boca Raton, 1994 ch. 23–25.
[11] M.A. Khan, et al., In-situ heavily *p*-type doping of over 10^{20} cm^{-3} in semiconducting $BaSi_2$ thin films for solar cells applications, Appl. Phys. Lett. 102 (2013) 112107.
[12] J. Derrien, J. Chevrier, V. Lethanh, J.E. Mahan, Semiconducting silicide-silicon heterostructures: growth, properties and applications, Appl. Surf. Sci. 56–58 (1992) 382–393.
[13] D. Tsukahara, et al., *p*-$BaSi_2$/*n*-Si heterojunction solar cells with conversion efficiency reaching 9.0%, Appl. Phys. Lett. 108 (2016) 152101.
[14] M Ramesh, M.K. Niranjan, Phonon modes, dielectric properties, infrared reflectivity and Raman intensity spectra of semiconducting silicide $BaSi_2$: a first-principles study, J. Phys. Chem. Sol. 121 (2018) 219–227.
[15] M. Ramesh, M.K. Niranjan, Theoretical investigation of lattice dynamics, dielectric properties, infrared reflectivity and Raman intensity spectra of Nowotny chimney ladder semiconducting silicide Ru_2Si_3, Mater. Chem. Phys. 222 (2019) 165–172.
[16] V.K. Zaitsev, et al., Highly effective $Mg_2Si(Sn)$ thermoelectrics, Phys. Rev. B 74 (2006) 045207.
[17] M. Akasaka, et al., The thermoelectric properties of bulk crystalline *n*- and *p*-type Mg_2Si prepared by the vertical Bridgman method, J. App. Phys. 104 (2008) 013703.
[18] W. Liu, et al., *n*-type thermoelectric material $Mg2Sn_{0.75}Ge_{0.25}$ for high power generation, PNAS 112 (2015) 3269.
[19] M. Mabuchi, K. Higashi, Strengthening mechanisms of Mg_2Si alloys, Acta Mater. 44 (1996) (1996) 4611.
[20] C. Li, X.F. Liu, G.H. Zhang, Mater. Sci. Eng. A 497 (2008) 432.
[21] J.E. Mahan, et al., Semiconducting Mg_2Si thin films prepared by molecular-beam epitaxy, Phys. Rev. B 54 (1996) 16965–16971.
[22] A. Vantomme, et al., Growth mechanism and optical properties of semiconducting Mg_2Si thin films, Microelectron. Eng. 50 (1 − 4) (2000) 237–242.
[23] T. Serikawa, et al., Depositions and microstructures of Mg-Si thin film by ion beam sputtering, Surf. Coat. Technol. 200 (2006) 4233–4239.
[24] S.W. Song, et al., Amorphous and nanocrystalline Mg_2Si thin-film electrodes, J. Power Sources 119-121 (2003) 110–112.
[25] N.G. Galkin, K.N. Galkin, S.V. Vavanova, Multilayer Si(111)/Mg_2Si Clusters/Si heterostructures: formation, optical and thermoelectric properties, E-J. Surf. Sci. Nanotechnol. 3 (2005) 12–20.
[26] F. Tran, P. Blaha, Phys. Rev. Lett. 102 (2009) 226401.
[27] H. Balout, P. Boulet, M.-C. Record, Thermoelectric properties of Mg_2Si thin films by computational approaches, J. Phys. Chem. C 118 (2014) 19635–19645.
[28] J.N. Liao, K. Li, F. Wang, X.S. Zeng, N.G. Zhou, Properties of Mg_2Si (100) surfaces: a first-principles study, Solid State Comm. 183 (2014) 41–46.
[29] D. Stradi, et al., General atomistic approach for modeling metal-semiconductor

interfaces using density functional theory and non-equilibrium Green's function, Phys. Rev. B 93 (2016) 155302.
[30] J. Heyd, G.E. Scuseria, M. Ernzerhof, J. Chem. Phys. 124 (2006) 219906.
[31] W. Kohn, L.J. Sham, Self-consistent equations including exchange and correlation effects, Phys. Rev. 140 (4A) (1965) A1133.
[32] J.M. Soler, E. Artacho, J.D. Gale, A. Garcıa, J. Junquera, P. Ordejon, D. Sanchez-Portal, J. Phys. Condens. Matter 14 (2002) 2745.
[33] Atomistix Toolkit Version 2018.1, Quantum Wise A/S (www.quantumwise.com).
[34] N. Troullier, J.L. Martins, Phys. Rev. B 43 (1991) 1993.
[35] D.M. Ceperley, B.J. Alder, Ground state of the electron gas by a stochastic method, Phys. Rev. Lett. 45 (1980) 566.
[36] P.E. Blöchl, Projector augmented-wave method, Phys. Rev. B 50 (1994) 17953.
[37] G. Kresse, J. Furthmüller, Efficient iterative schemes for ab initio total-energy calculations using a plane-wave basis set, Phy. Rev. B 54 (16) (1996) 11169.
[38] R.G. Morris, R.D. Redin, G.C. Danielson, Semiconducting properties of Mg_2Si single crystals, Phys. Rev. 109 (1958) 1909.
[39] J. Tejeda, M. Cardona, Valence bands of the Mg_2X (X = Si, Ge, Sn) semiconducting compounds, Phys. Rev. B 14 (1976) 2559.
[40] M.W. Finnis, V. Heine, Theory of lattice contraction at aluminum surfaces, J. Phys. F: Met. Phys. 4 (1974) 37.
[41] C. Nogiera, Physics and Chemistry at Oxide Surfaces, Cambridge University Press, 1996.
[42] J-h Cho, Ismail, Z. Zhang, E.W. Plummer, Oscillatory lattice relaxation at metal surfaces, Phys. Rev. B 59 (1999) 1677.
[43] M.K. Niranjan et al., Asymmetric-dimer reconstruction and semiconducting properties of Mg_2Si(100) surfaces: Prediction from meta-GGA and hybrid functional study, Solid State Sci., unpublished, In-press.
[44] K. Wandel (ed.), Surface and Interface Science, Vol. 1, Willey-VCH (2012).
[45] G.X. Qian, R.M. Martin, D.J. Chadi, First-principles study of the atomic reconstructions and energies of Ga- and As-stabilized GaAs(100) surfaces, Phys. Rev. B 38 (1988) 7649.
[46] K. Reuter, M. Scheffler, Composition, structure, and stability of RuO_2(110) as a function of oxygen pressure, Phys. Rev. B 65 (2001) 035406.
[47] M.K. Niranjan, L. Kleinman, A.A. Demkov, Electronic structure, elastic properties, surface energies, and work functions of NiGe and PtGe within the framework of density-functional theory for various surface terminations, Phys. Rev. B 75 (2007) 085326.
[48] R.M. Martin, Electronic Structure: Basic Theory and Practical Methods, CUP, 2004.
[49] M.K. Niranjan, Theoretical investigation of surface states and energetics of PtSi surfaces from first-principles density-functional theory, Surf. Sci. 649 (2016) 27–33.
[50] M.K. Niranjan, U.V. Waghmare, Relation between the work function and Young's modulus of RhSi and estimate of Schottky barrier height at RhSi/Si interface: an ab-initio study, J. Appl. Phys. 112 (9) (2012) 093702.
[51] M.K. Niranjan, Interface electronic structure and Schottky barrier heights in Si|NiSi (010) and Si|PtSi(010) heterostructures, Superlattices Microstruct. 100 (2016) 808–817.
[52] F.R. de Boer, et al., Cohesion in Metals, North-Holland, Amsterdam, 1988.
[53] G.H. Lu, et al., Relative stability of Si surfaces: A first-principles study, Surf. Sci. 588 (2005) 61–70.